Published online 21 July 2015 *Nucleic Acids Research, 2015, Vol. 43, No. 15* ***7489–7503***
doi: 10.1093/nar/gkv745

tRNA recognition by a bacterial tRNA Xm32 modification enzyme from the SPOUT methyltransferase superfamily

Ru-Juan Liu[1,2,†], Tao Long[1,2,†], Mi Zhou[1,2], Xiao-Long Zhou[1,2] and En-Duo Wang[1,2,3,*]

[1]State Key Laboratory of Molecular Biology, Institute of Biochemistry and Cell Biology, Shanghai Institutes for Biological Sciences, The Chinese Academy of Sciences, 320 Yue Yang Road, Shanghai 200031, China, [2]University of Chinese Academy of Sciences, Beijing 100039, China and [3]School of Life Science and Technology, ShanghaiTech University, 319 Yue Yang Road, Shanghai 200031, China

Received March 30, 2015; Revised July 8, 2015; Accepted July 12, 2015

ABSTRACT

TrmJ proteins from the SPOUT methyltransferase superfamily are tRNA Xm32 modification enzymes that occur in bacteria and archaea. Unlike archaeal TrmJ, bacterial TrmJ require full-length tRNA molecules as substrates. It remains unknown how bacterial TrmJs recognize substrate tRNAs and specifically catalyze a 2′-*O* modification at ribose 32. Herein, we demonstrate that all six *Escherichia coli* (*Ec*) tRNAs with 2′-*O*-methylated nucleosides at position 32 are substrates of *Ec*TrmJ, and we show that the elbow region of tRNA, but not the amino acid acceptor stem, is needed for the methylation reaction. Our crystallographic study reveals that full-length *Ec*TrmJ forms an unusual dimer in the asymmetric unit, with both the catalytic SPOUT domain and C-terminal extension forming separate dimeric associations. Based on these findings, we used electrophoretic mobility shift assay, isothermal titration calorimetry and enzymatic methods to identify amino acids within *Ec*TrmJ that are involved in tRNA binding. We found that tRNA recognition by *Ec*TrmJ involves the cooperative influences of conserved residues from both the SPOUT and extensional domains, and that this process is regulated by the flexible hinge region that connects these two domains.

INTRODUCTION

Post-transcriptional modifications frequently occur in RNA, notably in ribosomal RNA (rRNA), messenger RNA (mRNA), transfer RNA (tRNA), micro RNA and other small RNAs. Such modifications are essential for many important life processes (1–3). Among all of the known RNAs, tRNAs have the most modifications [see RNA modification and tRNA databases: http://modomics.genesilico.pl/ (4); http://rna-mdb.cas.albany.edu/RNAmods/ (5); http://trna.bioinf.uni-leipzig.de/ (6)], as more than 100 modifications have been identified in tRNA nucleosides (4), with the majority occurring in the main body and anticodon stem loop (ASL). Modifications in the ASL region usually improve tRNA–ribosome interactions and enhance translational efficiency and fidelity (7), but can also act as identity determinants for specific tRNA aminoacylation events (8).

Methylation is one of the most common and ubiquitous RNA modifications that can occur either on the base or the ribose of nucleosides (9). Most tRNA methylation reactions are catalyzed by S-adenosyl-L-methionine (SAM)-dependent methyltransferases (MTases). SAM-dependent MTases are can be grouped into five classes, among which methylating tRNAs belong to classes I and IV (9). Those MTases of class I contain a Rossmann fold in the catalytic domain (Rossmann fold MTases, RFM), whereas class IV MTases (also known as SPOUT MTases) contain a knotted domain. The SPOUT MTase superfamily was initially defined by bioinformatics studies based on the homology between the seemingly unrelated tRNA (Gm18) methyltransferases (SpoU, also named TrmH) and tRNA (m^1G37) methyltransferases (TrmD) (10). Subsequently, several crystallographic studies revealed that these SPOUT MTases all contain a common catalytic domain (SPOUT domain) that exhibits an unusual αβ-fold with a deep topological knot (11–15). Despite the high structural conservation of the SPOUT domain, the amino acid sequences are not conserved throughout the SPOUT superfamily (16). Hence, the specificity of substrate recognition for SPOUT MTases cannot be predicted based on sequence homology alone. Although many SPOUT MTases harbor N- or C-terminal extensions for substrate RNA binding on their conserved SPOUT domain (16), a group of minimalist SPOUT proteins remains that includes TrmL [tRNA (Um34/Cm34)

*To whom correspondence should be addressed. Tel: +86 21 54921241; Fax: +86 21 54921011; Email: edwang@sibs.ac.cn
†These authors contributed equally to the paper as first authors.

MTase] (17,18) and the rRNA-specific RlmH subfamily (19,20), which are restricted to the unique catalytic SPOUT domain.

Despite enormous structural diversity, MTases specifically modify RNA nucleosides at defined positions. Normally, recognition of substrate tRNAs occurs in one of two ways, either by protein-only MTases or by ribonucleoprotein complexes in which a small C/D box RNA guides the MTase to the target nucleoside (21–24). To date, all SPOUT MTases investigated utilize the protein-only mechanism. In the absence of SPOUT/RNA complexes, substrate recognition has been primarily studied using biochemical methods, most often on proteins from the TrmD [tRNA(m^1G37) MTases] (25–30) and TrmH [tRNA(Gm18) MTases] (31–34) families. Thus, tRNA substrates are recognized by protein surface residues from both the SPOUT and extension domains. A recent study suggested that TrmH discriminates between tRNA substrates based on the catalytic domain rather than on extension stretches (34). Similarly, recognition of tRNA by the minimalist SPOUT MTase TrmL was shown to occur on the protein surface via basic amino acid residues from the SPOUT homodimer (18).

Methylation of ribose moieties in tRNA is frequent, especially at position 32 where it is commonplace in all three domains of life (9). In eukarya, methylation is performed by Trm7 MTases from the RFM superfamily (35) and, as shown for yeast Trm7, methylation requires the assistance of an auxiliary protein, Trm732 (36,37). SPOUT MTases TrmJ (abbreviated as tRNA [Xm32] MTases, with X representing any nucleoside) are specific to archaea and bacteria (38,39). Archaeal TrmJ from *Sulfolobus acidocaldarius* (*Sa*) has a narrow specificity and only methylates C32 (39), in contrast to bacterial TrmJ from *Escherichia coli* (*Ec*) that can methylate all four nucleosides at position 32 (39), even though A and G residues are rare or absent at position 32 in the anticodon loop of tRNA (6). Moreover, a mutational analysis of tRNA variants for methylation by these two homologous TrmJs indicated that *Ec*TrmJ likely requires a full-length tRNA, in contrast to *Sa*TrmJ that can methylate tRNA fragments that lack a D- and T-stem/loop (39). Specifically, the identity of the D-stem and D-loop, but not the anticodon loop, is critical for tRNA recognition by *Ec*TrmJ. However, the mechanisms of tRNA discrimination and methylation by bacterial and archaeal TrmJ MTases remain unclear (39).

The dependence of full-length tRNA for the methylation capacity of bacterial TrmJ MTases is intriguing, because other bacterial tRNA MTases from the SPOUT superfamily show less stringent specificity for the tRNA architecture. This applies to 2′-*O* ribose MTases that are specific for position G18 (e.g. *Thermus thermophilus* TrmH) and MTases from the TrmD subfamily (e.g. *Ec*TrmD) that catalyze the formation of m^1G37, as these enzymes are structurally related to TrmJ MTases; both enzymes can catalyze either the formation of Gm18 in 5′-half-fragments of tRNA, although with low efficiency (TrmH) (40), or of m^1G37 in ASL domains (TrmD) (27). Intriguingly, the formation of Cm34/Um34 by *Ec*TrmL, another bacterial SPOUT MTase, can catalyze the modification of isolated ASL domains with certain sequence and post-transcriptional modifications, such as the i^6 modification at A37 (17,18,41).

In summary, many intriguing questions regarding how SPOUT MTases specifically recognize and methylate tRNA substrates remain unanswered, despite the abundance of structural and functional studies described above. Herein, we examined the mechanism of tRNA recognition by *Ec*TrmJ. To gain further insights into this mechanism, we used a variety of experimental approaches to study the methylation of the six *Ec*tRNAs with a 2′-*O* methylated nucleoside at position 32, and solved the first full-length crystal structure of *Ec*TrmJ in complex with SAH (S-adenosylhomocysteine), the demethylated SAM. We show that all six tRNAs are efficiently methylated by the cognate *Ec*TrmJ, which behaves as an unusual asymmetric dimer either in crystal or in solution. We further characterize nucleosides in tRNAs and amino acids in *Ec*TrmJ that are essential for methylation. Overall, our data indicate that the L-shaped tRNA fold, but not the integrity of the acceptor stem is required by *Ec*TrmJ and both the catalytic N-terminal and extensional C-terminal domains (NTD and CTD, respectively) of *Ec*TrmJ play key roles in tRNA binding and methylation. The functional role of *Ec*TrmJ is discussed in the light of the structure–function relationships that have been described for other SPOUT MTases.

MATERIALS AND METHODS

Materials

SAM, SAH, 5′-GMP, Tris-base, β-mercaptoethanol (β-Me), KCl and the reagents used to optimize crystallization conditions were purchased from Sigma–Aldrich (St Louis, MO, USA). $MgCl_2$, NaCl, adenosine triphosphate, cytidine triphosphate, guanosine triphosphate and uridine triphosphate were from Sangon Biotech (Shanghai, China). [Methyl-^{3}H] SAM was obtained from PerkinElmer (Waltham, MA, USA); crystallization kits were from Hampton research (Aliso Viejo, CA, USA). Primers for polymerase chain reaction were synthesized by Invitrogen (Shanghai, China) and Biosune (Shanghai, China); the pET22b vector was from Merck–Millipore (Darmstadt, Germany). The KOD-plus mutagenesis kit, Pyrobest DNA polymerase and dNTP mixture were obtained from Takara (Shiga, Japan); T4 ligase and other restriction endonucleases were obtained from MBI Fermentas (Pittsburgh, PA, USA). Pyrophosphatase (PP_iase) was purchased from Roche Applied Science (Basel, Switzerland). Ni^{2+}-NTA Superflow was obtained from Qiagen (Dusseldorf, Germany). The Superdex 200 column and 3 mm filter papers were from GE Healthcare (Fairfield, CT, USA). The analog of SAM, sinefungin, was purchased from Santa Cruz Biotechnology (Santa Cruz, CA, USA).

Cloning, mutagenesis and gene expression, and protein characterization

The gene encoding *Ec*TrmJ was amplified from the *E. coli* K-12 MG1655 genome and cloned into vector pET22b at the *Nde*I and *Xho*I sites with a C-terminal His_6-tag. Genes encoding the various mutants, including single site mutants, Δ2 (delete residues 171–172), Δ4 (delete residues 171–174), Δ7 (delete residues 169–175), Δ10 (delete residues

167–176), Δ12 (delete residues 166–177), NTD (residues 1–170) and CTD (residues 171–246) was performed using the KOD-plus mutagenesis kit according to the manufacturer's instructions (Supplementary Table S1). All constructs were confirmed by DNA sequencing and expressed in *E. coli* BL21 (DE3). Proteins were purified by affinity chromatography on a Ni^{2+}-NTA Superflow resin followed by gel filtration chromatography with a Superdex^{TM} 200 column (10/300 GL; column volume, 23.562 ml) (Supplementary Figure S1). The protein concentrations were determined by UV absorbance at 280 nm, and the molar absorption coefficient was calculated according to the sequence of each protein (42). The concentration of each protein refers to monomer concentration.

Preparation of tRNAs

Gene sequences of *Ec*tRNA$^{Gln}_1$(UUG), *Ec*tRNA$^{Gln}_2$(CUG), *Ec*tRNA$^{Ser}_1$(UGA), *Ec*tRNA$_f^{Met}_1$(CAU), *Ec*tRNA$_f^{Met}_2$(CAU) and *Ec*tRNA$^{Trp}_1$(CCA) were obtained from the MODOMICS database (1) and cloned between the *Eco*RI and *BamH*I sites of pTrc99b with a 5′-terminal T7 promoter. Mutants of the *Ec*tRNA$_f^{Met}_1$ genes were generated using the KOD-plus mutagenesis kit. All tRNAs were generated by *in vitro* transcription using T7 RNA polymerase, as described previously (18). The tRNA concentrations were determined by UV absorbance at 260 nm, and the molar absorption coefficient was calculated according to the sequence of each tRNA (43).

Measurements of methyltransferase activity

Standard assays for methyltransferase activity of wild-type and mutant *Ec*TrmJs were conducted as follows: 0.5 μM protein, 5 μM tRNA and 100 μM [Methyl-^{3}H]SAM in buffer [50 mM Tris–HCl (pH 9.0), 100 mM KCl, 10 mM $MgCl_2$]. Reaction mixtures were incubated for various time intervals at 37°C and then aliquots were spotted on filters and quenched by 5% trichloroacetic acid. The amount of radioactive [^{3}H]-methyl-tRNA was measured using a Beckman Ls6500 scintillation counting apparatus. A range of 0.25–30 μM tRNA and 0.2 μM *Ec*TrmJ were used to determine the kinetic parameters of the methylation reactions. For mutants that exhibit extremely low activities, higher concentrations of enzyme and tRNA substrates were used. The kinetic parameters, K_m and k_{cat}, of the methyl transfer reaction with [Methyl-^{3}H]SAM were determined using Lineweaver–Burk plots.

Crystallization, structure determination and structure refinement

Purified *Ec*TrmJ in buffer A (20 mM Tris-HCl, pH 7.5; 100 mM NaCl; 10 mM $MgCl_2$) was concentrated to 10 mg/ml for crystallization. A final concentration of 2 mM SAH was added to the *Ec*TrmJ protein solution to make a mixture for drop setting. The initial crystallization conditions were screened using Crystal Screen 2^{TM} (Hampton Research; Aliso Viejo, CA, USA). After modifying the conditions, good crystals of *Ec*TrmJ–SAH complexes were obtained by hanging drop vapor diffusion at 20°C after 2 months under conditions of 3.6 M NaCl and 0.1 M 4-(2-Hydroxyethyl)-1-piperazineethane sulfonic acid (HEPES, pH 8.2).

Crystals were mounted on a nylon loop and flash-cooled into a liquid N_2 stream using paraffin oil as a cryoprotectant. The crystal diffraction dataset was collected at the Shanghai Synchrotron Radiation Facility (SSRF) beamline BL-17U1 at 100 K. Diffraction data were processed using the HKL2000 software package (44).

The structure of the *Ec*TrmJ–SAH complex was solved by molecular replacement with the PHASER program (45) in the CCP4 suite (46) using the structure of a hypothetical MTase from *Haemophilus influenzae* (PDB ID: 3ILK) as the initial search model. The model was improved by automatic building using PHENIX (47) and manual adjustments were made with COOT (48). Structure refinement was performed using the programs REFMAC5 (49) and PHENIX (47). Throughout the refinement process, 5% of randomly chosen reflections were set aside for free *R* factor monitoring. The quality of the final model was evaluated using PROCHECK (50) from the CCP4 software suite. All structure figures were generated using PyMOL (http://www.pymol.org) and the figure for the secondary structure-based sequence alignment was made using the ENDscript server (51).

Electrophoretic mobility shift assays (EMSAs)

Purified protein (final concentrations, 0, 0.25, 0.75, 1, 1.5, 2, 4, 8 and 16 μM), 200 nM *Ec*tRNA$_f^{Met}_1$ transcript and 500 μM sinefungin (a stable analog of SAM, also known as adenosyl-ornithine) were incubated in 21 μl buffer B [50 mM Tris–HCl (pH 8.0), 100 mM NaCl, 5 mM $MgCl_2$ and 20% glycerol] at 37°C for 10 min. After incubation, 2 μl loading solution (0.25% bromophenol blue, 0.25% xylene cyanide and 30% glycerol) were added into each sample and loaded immediately on a 6% polyacrylamide native gel, which was prepared with 50 mM Tris-glycine buffer (pH 8.5). Electrophoresis was carried out on ice at a constant voltage of 65 V for 80 min. Ethidium bromide and Coomassie brilliant dye were used to stain the gel to detect RNA and protein, respectively. RNA bands were quantified using a Fuji Film imaging analyzer.

Isothermal titration calorimetry (ITC) measurements

Isothermal titration calorimetry (ITC) measurements were performed using an ITC200 Micro-calorimeter (MicroCal Inc.; Studi City, CA, USA) at 25°C. Samples were buffered with 20 mM Tris–HCl (pH 7.5) containing 100 mM NaCl and 10 mM $MgCl_2$. Aliquots of 1 mM SAH solutions (syringe) were injected step-wise into a 60 μM protein solution (cell). SAH titrated in an identical buffer was used as a control. Data were subsequently analyzed and fitted using a one set of sites model using Origin Software version 7.0 (MicroCal Inc.).

RESULTS

The tRNA substrates of *Ec*TrmJ

A total of six tRNAs from *E. coli* have 2′-*O*-methylated nucleosides at position 32, as presented in the MODOMICS

database (1). They are $tRNA^{Gln}_1$(UUG), $tRNA^{Gln}_2$(CUG), $tRNA^{Ser}_1$(UGA), $tRNA_f{}^{Met}_1$(CAU), $tRNA_f{}^{Met}_2$(CAU), and $tRNA^{Trp}_1$(CCA) (Figure 1A). In this present study, we transcribed all six candidate tRNAs *in vitro* and measured their methylation catalyzed by *Ec*TrmJ. Furthermore, $tRNA^{Gln}_2$ and $tRNA^{Ser}_1$ had been previously identified as substrates of *Ec*TrmJ (38,39), and the other four candidates could also be methylated by *Ec*TrmJ (Figure 1B and C). Therefore, all of these six tRNAs are substrates of *Ec*TrmJ. Subsequently, we measured the steady-state kinetic parameters of *Ec*TrmJ for these six substrates (Table 1). According to the kinetic parameters of methylation, the tRNA substrates could be divided into two groups as follows: Group 1 with $tRNA_f{}^{Met}_1$, $tRNA_f{}^{Met}_2$, and $tRNA^{Trp}_1$ where K_m values were all below 1 μM and k_{cat} values ranged from 1.31 to 1.52 min^{-1}, and Group 2 with $tRNA^{Gln}_1$, $tRNA^{Gln}_2$, and $tRNA^{Ser}_1$, characterized by higher K_m values >5 μM and k_{cat} values that were similar to those of Group 1 (Table 1). Collectively, our data show that all six *Ec*tRNAs with a methylated 2′-*O*-ribose at position 32 are substrates of *Ec*TrmJ. In the following experiments, we chose to study $tRNA_f{}^{Met}_1$, which has a lower K_m value, to characterize tRNA recognition by *Ec*TrmJ.

The L-shaped tertiary structure of tRNA is essential for recognition by *Ec*TrmJ

In a previous study, it was shown that *Ec*TrmJ requires full-length tRNA molecules as substrates, and that the identity of the D-stem and D-loop, but not the anticodon loop, is important for recognition by *Ec*TrmJ (39). To obtain insights into the details of tRNA recognition by *Ec*TrmJ, we furthered those studies by investigating the roles of the acceptor stem and elbow region. First, we truncated the acceptor stem in a step-wise manner (Figure 2A and Table 2) and, surprisingly, found that *Ec*TrmJ could transfer the methyl group from SAM to those truncated tRNAs, unless the whole acceptor stem was completely deleted (Figure 2B). Then, we disrupted the L-shaped tertiary structure of tRNA by introducing single mutations into the elbow region (within D- and T-loops) of G18–U55 or G19–C56 (Figure 2A), which showed that all of these tRNA mutants could no longer be catalyzed by *Ec*TrmJ (Figure 2C). Consistently, when we made double-mutations to restore the L-shape tertiary structure of tRNA by keeping the two hydrogen bonds in the U18–G55 region, the mutant tRNA could again be methylated by *Ec*TrmJ (Figure 2C and Table 2). Overall, our results show that the L-shaped tertiary structure of tRNA is essential for recognition by *Ec*TrmJ, while the acceptor stem region is not involved in this process.

Crystal structure of *Ec*TrmJ

We attempted to crystallize the *Ec*TrmJ-tRNA complex to understand the mechanism of tRNA recognition; however, we only obtained crystals of *Ec*TrmJ with a bound SAH. The final model of the *Ec*TrmJ–SAH binary complex (PDB ID: 4XBO) was refined to 2.6 Å. Data collection parameters and refinement statistics are summarized in Table 3. The space group is $C222_1$, and one asymmetric unit contains two *Ec*TrmJ molecules. In the crystal structure of *Ec*TrmJ, each subunit contains two domains connected by a linker region. The structure of NTD presents as a typical SPOUT fold structure with a deep trefoil knot (Figure 3A). The CTD is a helix bundle composed of three anti-parallel helices (Figure 3A). The linker of 16 residues (164–179) connecting the NTD and CTD is largely invisible in the electron density map of both monomers in the asymmetric unit (Figure 3A). To check whether the crystals contained full-length *Ec*TrmJ protein or separate NTD and CTD domains, we analyzed dissolved crystals by SDS–PAGE. Our data clearly showed that crystals contained full-length *Ec*TrmJ protein molecules (Supplementary Figure S2). Thus, the missing density in the electron density map indicates an intrinsic flexibility of the linker region. The crystal structure of *Ec*TrmJ corresponds to a dimer (Figure 3A), consistent with the state of *Ec*TrmJ in solution, as determined by analytical gel filtration (data not shown). Based on a view of sequence, *Ec*TrmJ dimer exists as a homodimer. However, the conformation of the two subunits of the *Ec*TrmJ dimer are different (Figure 3A), especially the relative orientations between the CTD and NTD domains (Figure 3B), which suggest that *Ec*TrmJ forms an unusual asymmetric dimer.

The overall structure of NTD (residues 1–164) within the full-length *Ec*TrmJ is quite similar to that of the previously reported crystal structure of isolated NTD ($EcTrmJ_{1–164}$; PDB: 4CNE) (39) generated during the crystallization of the full-length protein (39), and only few variations distinguished the structures of the two NTD versions. The NTD is composed of six β-strands and six α-helices, in the order β1-α1-β2-α2-β3-α3-β4-α4-β5-α5-β6-α6 (Figure 3A and C). The parallel six-stranded β-sheet is flanked by four α-helices on one side and by two α-helices on the other side (Figure 3A). The C-terminal part of NTD forms a deep trefoil knot and the SAH is bound in this knot region (Figure 3A). Compared with the structure of the isolated NTD, the main difference is from residues 41–50, which linked β2 and α2; in our present structure this was a long loop in one subunit and disordered in the other subunit. By contrast, in the isolated NTD, this region forms an α-helix in one subunit and is similarly disordered in the other subunit. Architecturally, the SPOUT fold NTD forms a dimer in a 'perpendicular' mode (Figure 3A), which is similar to the structure reported for the SpoU MTases TrmL and TrmH (14,15,18).

SAH is bound to the knotted region of NTD. The SAH binding pocket is robustly formed by residues from three loops, including the beginning of loops β4-α4, β5-α5, and β6-α6 (Figures 3A and 4A). Indeed, the formation of the SAM/SAH-binding pocket is highly conserved in all of the reported SPOUT MTases, which all involved those three loops. The primary amino acid sequences are not well conserved in all SPOUT MTase family members. Only three relatively conserved motifs (motif I, II, and III) were identified (31), and two of those three motifs, motif II (loop β5-α5) and motif III (loop β6-α6), are involved in SAM/SAH binding. Residues from these two loops can promiscuously interact with the SAH, as shown in detail in Figure 4B. In the case of loop β4-α4, only the initial three residues were involved in SAH binding (Figure 4A and B). Interestingly, residues from loop β4-α4 are not conserved in

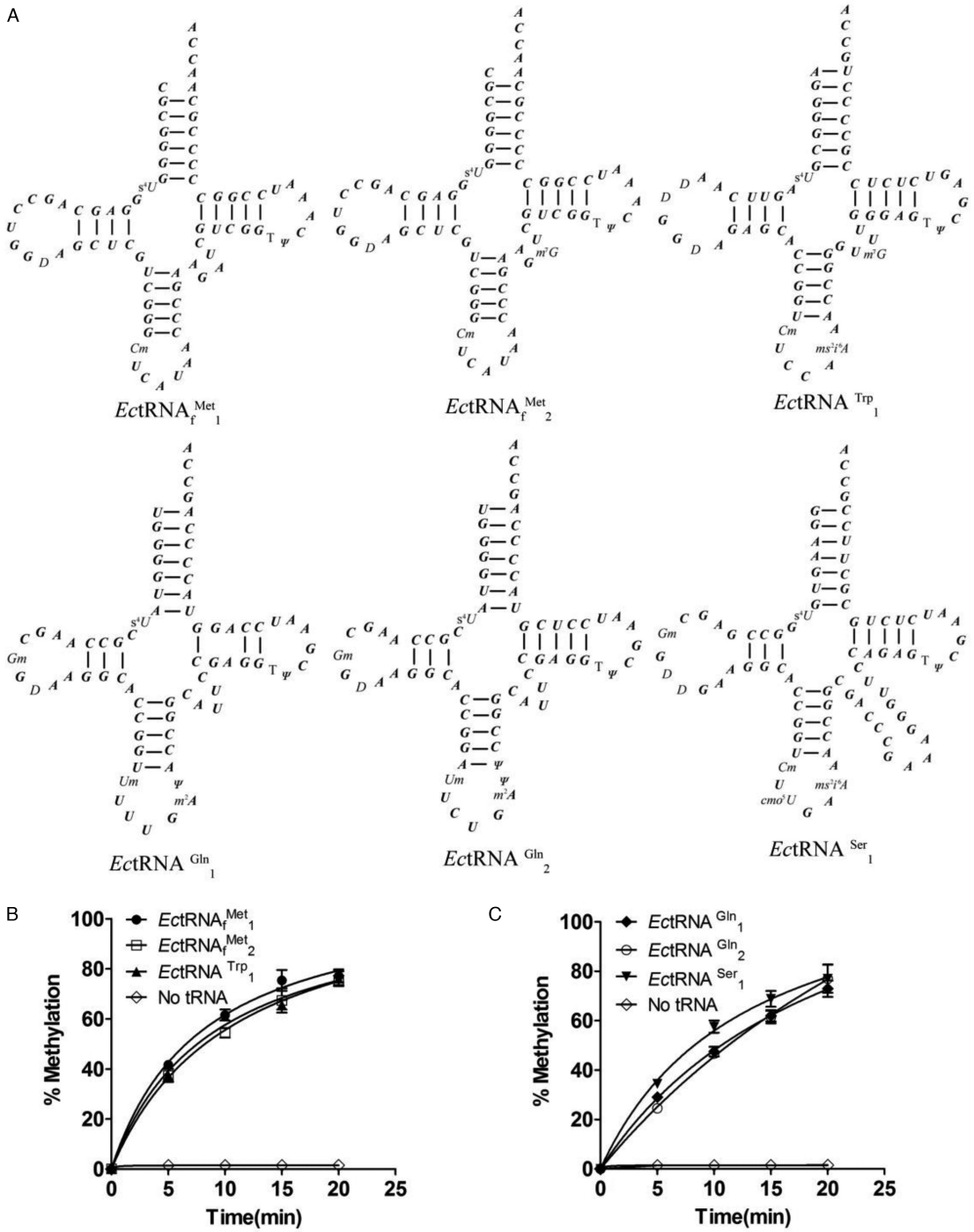

Figure 1. The tRNA substrates of TrmJ in *Escherichia coli*. (**A**) The cloverleaf structures of six *E. coli* tRNAs with a 2′-*O*-methylated ribose in position 32 from the MODOMICS database. (**B** and **C**) The methyltransferase activity of *Ec*TrmJ for tRNA substrates. Error bars represent standard errors of three independent experiments.

SPOUT MTases. In TrmD, TrmH, and TrmL, loop β4-α4 is composed of 6 to 8 amino acid residues. However in TrmJ, loop β4-α4 is much longer, and contains 14 to 16 amino acid residues; in *Ec*TrmJ, loop β4-α4 is 15 amino acids long from residues 79–93 (Figure 3C). Based on the sequence alignment (Figure 3C), the first half of loop β4-α4 is conserved among bacterial TrmJs with a 'TXARXR' motif (Figure 3C), which we designate here as the 'TrmJ-specific motif'. Residues ^{79}TSA^{81} from this 'TrmJ-specific motif' of *Ec*TrmJ all can directly interact with SAH (Figure 4A and B).

The overall structure of the CTD of *Ec*TrmJ is a three-helix fold organized in an α7-α8-α9 bundle, with the three helices oriented anti-parallel to each other (Figures 3A and

Table 1. Kinetic parameters of *Ec*TrmJ for various tRNA substrates for the methyl-transfer reaction

tRNAs	K_m (μM)	k_{cat} (min^{-1})	k_{cat}/K_m
*Ec*tRNA$_f^{Met}{}_1$(CAU)	0.67 ± 0.06	1.52 ± 0.08	2.28
*Ec*tRNA$_f^{Met}{}_2$(CAU)	0.81 ± .04	1.42 ± 0.18	1.75
*Ec*tRNA$^{Trp}{}_1$(CCA)	0.94 ± 0.07	1.31 ± 0.07	1.40
*Ec*tRNA$^{Gln}{}_1$(UUG)	9.88 ± 0.55	1.20 ± 0.10	0.12
*Ec*tRNA$^{Gln}{}_2$(CUG)	5.79 ± 0.95	1.41 ± 0.13	0.24
*Ec*tRNA$^{Ser}{}_1$(UGA)	11.82 ± 1.34	2.30 ± 0.13	0.19

Data indicate means from three independent measurements.

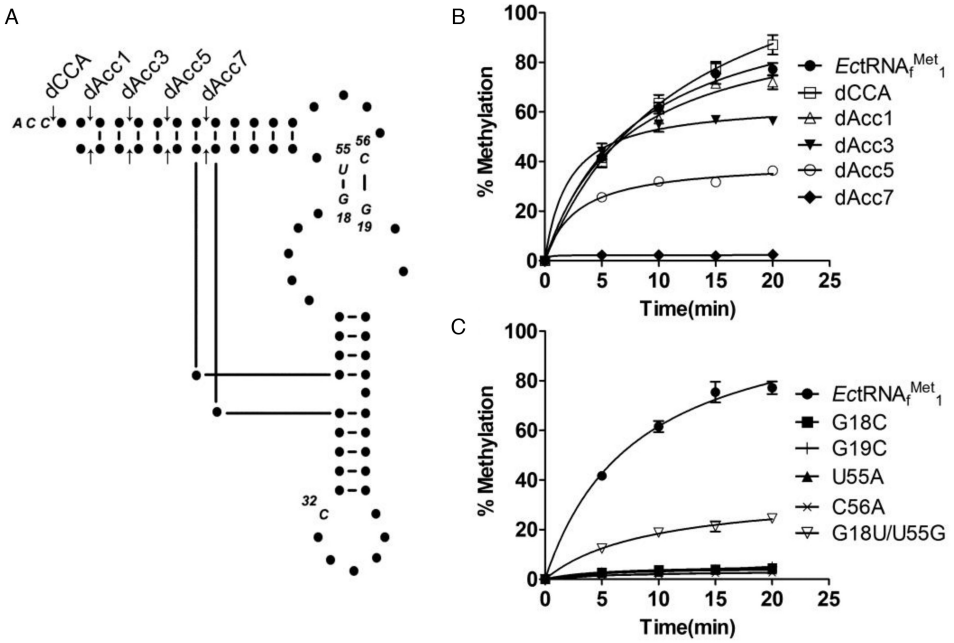

Figure 2. Recognition of tRNA elements by *Ec*TrmJ. (**A**) A model of L-shaped *Ec*tRNA$_f^{Met}{}_1$ with arrows showing truncations on the acceptor stem. (**B**) The methyltransferase activity of *Ec*TrmJ for *Ec*tRNA$_f^{Met}{}_1$ and its various truncations. (**C**) The methyltransferase activity of *Ec*TrmJ for *Ec*tRNA$_f^{Met}{}_1$ and its mutations on the elbow region. Error bars represent standard errors of three independent experiments.

Table 2. Kinetic parameters of *Ec*TrmJ for *Ec*tRNA$_f^{Met}{}_1$(CAU) variants for the methyl transfer reaction

Variants	K_m (μM)	k_{cat} (min^{-1})	k_{cat}/K_m (relative)
wild-type	0.67 ± 0.06	1.52 ± 0.08	1
dCCA	0.61 ± 0.04	1.40 ± 0.08	1.00
dAcc1	0.74 ± 0.05	1.52 ± 0.08	0.89
dAcc3	0.88 ± 0.08	1.44 ± 0.01	0.71
dAcc5	1.37 ± 0.18	1.26 ± 0.06	0.40
dAcc7	ND	ND	ND
G18U/U55G	9.92 ± 1.62	1.34 ± 0.05	0.06

Data indicate means from three independent measurements; ND, not detectable.

4C). Interestingly, this CTD in the crystal structure also forms a dimer, which is consistent with the dimerization state of an isolated CTD in solution, as identified by SAXS (39). Extension domains exist widely in SPOUT proteins, such as TrmH and TrmD; however, none of those reported extension domains have been previously observed to form a dimer (11–13,15). In *Ec*TrmJ, residues from loop α7-α8 and helix α8 interact widely with residues from helix α9' of the other subunit to form the CTD dimer (Figure 4C). Interestingly, most of these residues are conserved in the TrmJ family (Figure 3C), which suggests that CTD dimerization is conserved. To identify the function of those residues, we mutated the conserved amino acids F199, E225, I228, L229, and G231 to Ala, as shown in Figure 4D. These mutants either totally abolished (E225A, L229A, and G231A) or largely reduced (F199A and I228A) the catalytic activity of *Ec*TrmJ. These results suggest that the dimerization of CTD is important for the catalytic activity of *Ec*TrmJ.

To gain insights into the possible tRNA binding regions in *Ec*TrmJ, the protein surface electrostatic potential map that we generated is shown in Figure 4E. We observed two large positively charged surface patches that formed

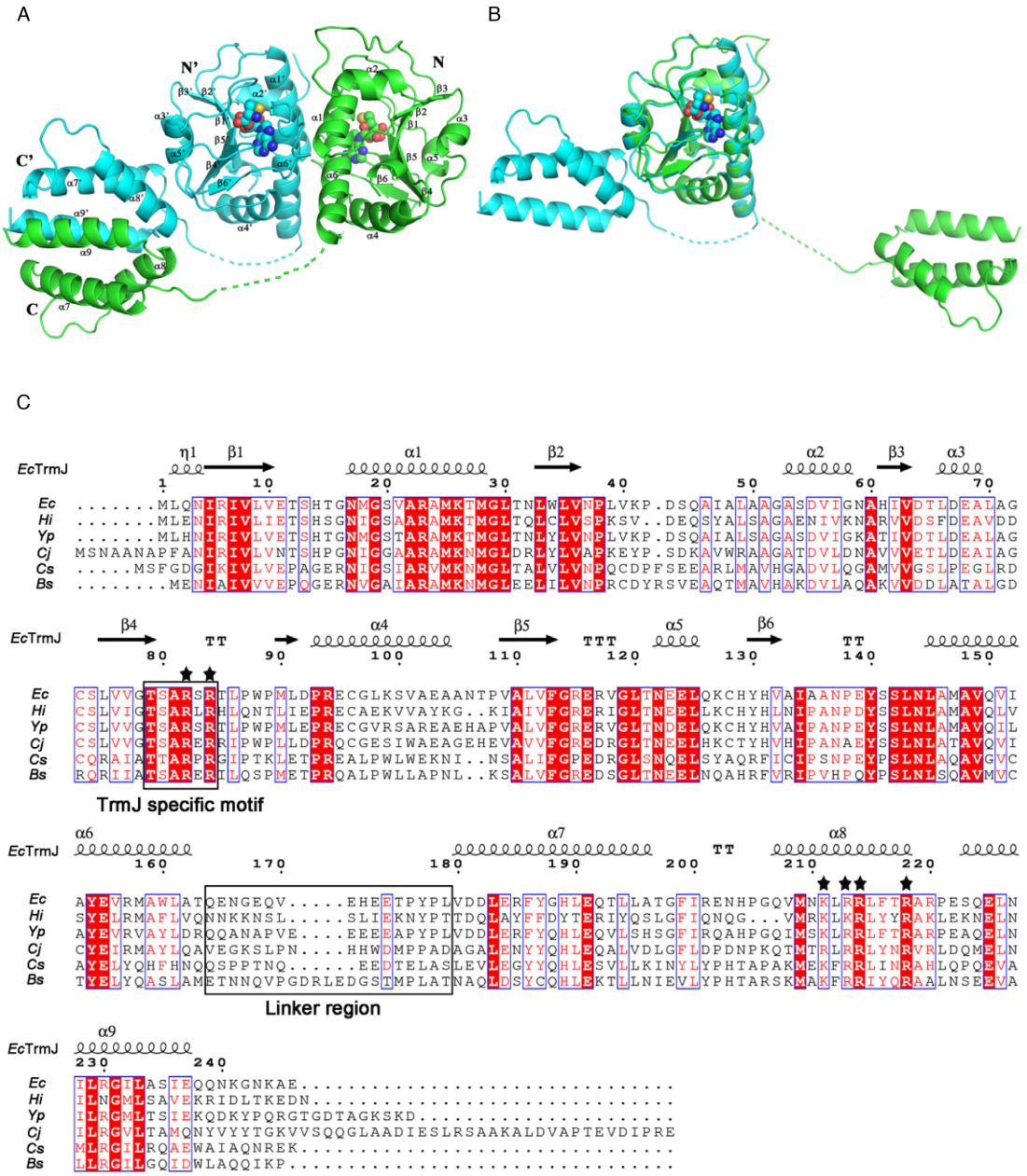

Figure 3. The overall structure of the *Ec*TrmJ–SAH complex and a sequence alignment of bacterial TrmJs. (**A**) A ribbon diagram shows the overall structure of *Ec*TrmJ in complex with SAH (presented in spheres). The structure is shown as a dimer, with one subunit in green and the other one in cyan. The invisible linker regions are shown as dotted lines. (**B**) An overlay of the two monomers (cyan and green) in the asymmetric *Ec*TrmJ dimer that superposition the SPOUT domains alone. The spheres represent bound SAH. (**C**) A structure-based multiple amino acid sequence alignment of bacterial TrmJs from model organisms. Abbreviations used: *Ec*, *Escherichia coli*; *Hi, Haemophilus influenza*; *Yp*, *Yersinia pestis*; *Cj*, *Cellvibrio japonicas*; *Cs*, *Cyanobacteriumstanieri*; and *Bs*, *Bacillus subtilis*. The secondary structure elements of *Ec*TrmJ are labeled above the alignment. Residues involved in tRNA binding that were identified in this study are marked by a black pentagon.

from each subunit, with one located near the SAH binding pocket, which mainly includes residues R82 and R84 from the 'TrmJ-specific motif' in loop β4-α4 and residues R115 and R117 from loop β5-α5, and the other patch is in the CTD, composed of the basic residues K211, R213, R214, and R218 from helix α8. In the following sections, we examine whether each of these residues is involved in tRNA binding.

Conserved basic residues from the 'TrmJ-specific motif' are involved in tRNA binding

We first focused on the large positively charged surface patch around the SAH binding pocket composed of arginine residues (R82, R84, R115 and R117) that are conserved in bacterial TrmJs, except for R117. Therefore, we mutated R82, R84, and R115 to alanine respectively to perform electrophoretic mobility shift assay (EMSA) and

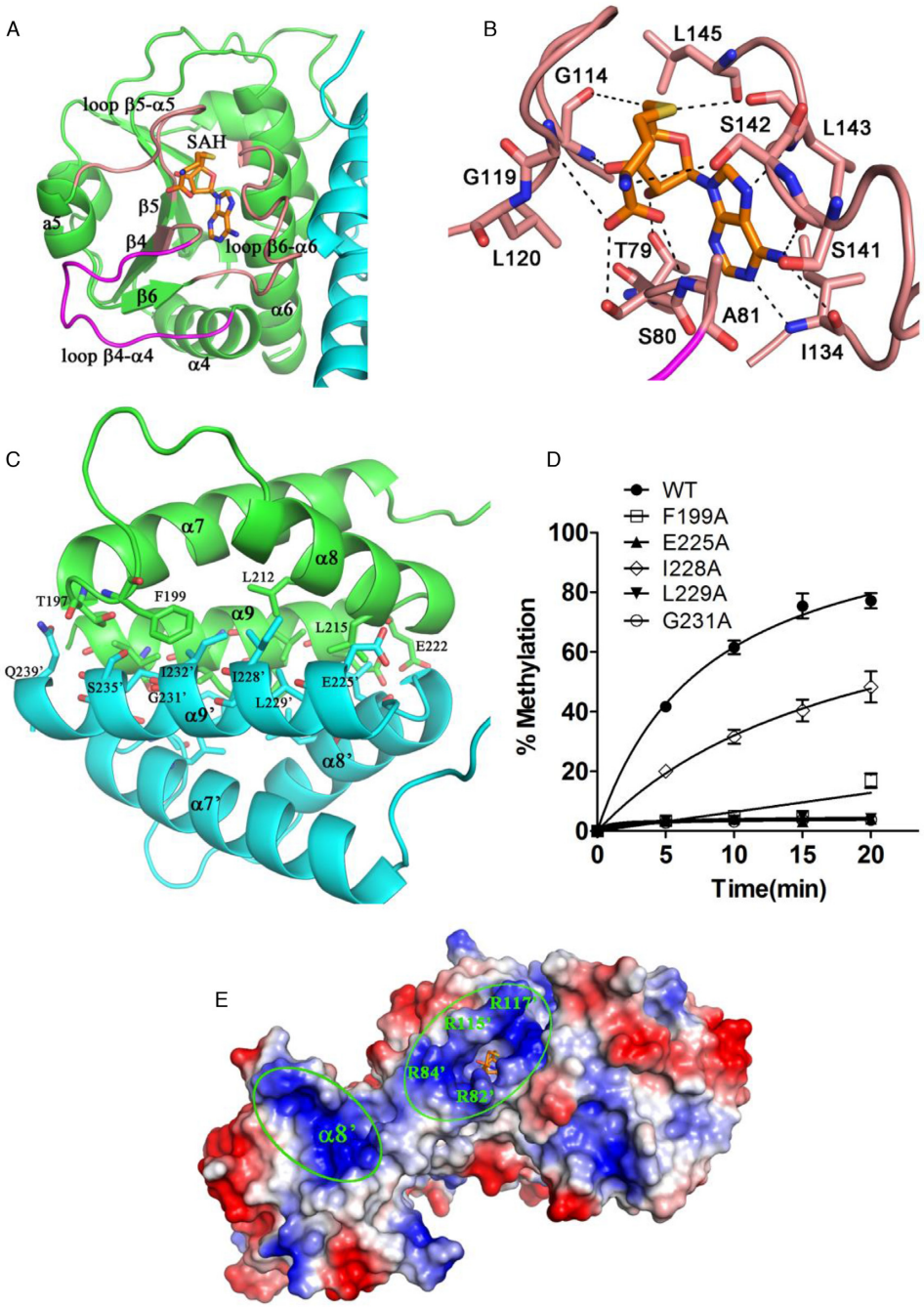

Figure 4. Structural details of the *Ec*TrmJ–SAH complex. SAH bound in one subunit of *Ec*TrmJ (**A**) and all residues within 4 Å from SAH are shown as a stick (**B**). The carbon atom of SAH is shown in orange, the backbone of *Ec*TrmJ and the SAH-binding pocket are shown in green and salmon, respectively, and part of the loop β4–α4 that contained residues R82 and R84 is shown in magenta. (**C**) A ribbon diagram showing the CTD dimer, residues at the dimer interface are shown as sticks. (**D**) The methyltransferase activities of various *Ec*TrmJ mutants. Error bars represent standard errors of three independent experiments. (**E**) The vacuum electrostatics of *Ec*TrmJ; two large positively charged patches are circled in green.

ITC assays. In a preliminary experiment, we first used EMSA to analyze the binding affinity of tRNA for wild-type *Ec*TrmJ. To our surprise, no tRNA–enzyme complex band could be observed, even after optimizing the binding conditions using different tRNA substrates, different pH levels or different concentrations of SAM and SAH. However, only after the SAM analog sinefungin was introduced into the binding solution, a stable tRNA–enzyme complex band appeared on the gel. Therefore, all subsequent EMSAs were performed in the presence of 500 μM sinefungin and 200 nM $tRNA_f^{Met}{}_1$ (Figure 5A). For wild-type *Ec*TrmJ, a shift was observed starting at 0.25 μM enzyme, which represented the *Ec*TrmJ–tRNA complex (tRNA-bound). The K_d value was calculated by quantifying the bound tRNAs, which yielded an apparent K_d value of ∼1.0 μM. The tRNA binding affinities of *Ec*TrmJ mutants

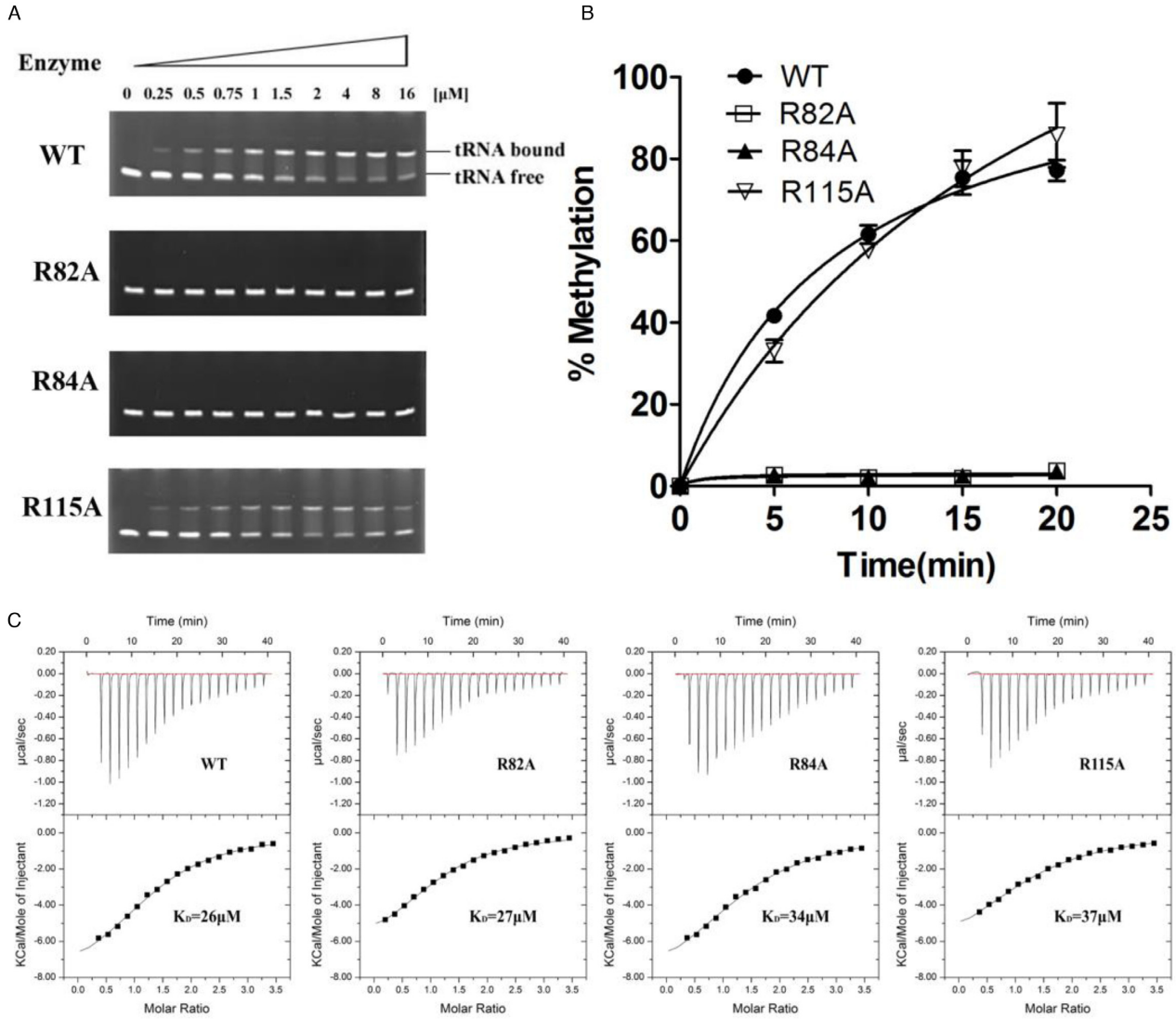

Figure 5. Ala mutations of basic amino acid residues near the SAM/SAH-binding pocket of *Ec*TrmJ. (**A**) The binding affinities of *Ec*TrmJs for *Ec*tRNA$_f^{Met}{}_1$ were analyzed using a gel mobility shift assay. (**B**) Methyltransferase activities of various *Ec*TrmJ mutants. Error bars represent standard errors of three independent experiments. (**C**) The SAH binding affinity, as measured by ITC.

are compared in Figure 5A. *Ec*TrmJ-R82A and *Ec*TrmJ-R84A totally lost tRNA binding affinity under these conditions, while the *Ec*TrmJ-R115A mutant showed similar binding affinity to wild-type *Ec*TrmJ. We further assayed the activity of the methyltransferase and its mutants (Figure 5B). Consistently, *Ec*TrmJ-R82A and *Ec*TrmJ-R84A totally lost their activity, but *Ec*TrmJ-R115A exhibited high enzymatic activity, similar to wild-type *Ec*TrmJ (Table 4). Since EMSA was operated in the presence of a SAM analog, the possibility that the *Ec*TrmJ-R82A and *Ec*TrmJ-R84A mutants abolished SAM/SAH binding capability should be excluded first. Thus, ITC was applied to assay the SAH binding affinity of *Ec*TrmJs (Figure 5C). We found that *Ec*TrmJ-R82A, *Ec*TrmJ-R84A and *Ec*TrmJ-R115A all had dissociation constants (K_D) for SAH that were comparable to *Ec*TrmJ. These findings suggest that defects in the methyltransferase activity of *Ec*TrmJ-R82A and *Ec*TrmJ-R84A were not caused by reduced SAM/SAH binding, but instead resulted from perturbed tRNA binding capability.

Basic residues of CTD on the protein surface are involved in tRNA binding

We next focused on the second large positively charged surface patch in the CTD of *Ec*TrmJ. Interestingly, this patch is mainly formed by residues K211, R213, R214 and R218 from the solvent surface of helix 8 (Figure 4E), and the opposite surface of this helix is involved in dimer formation of the CTD (Figure 4C). These four residues—K211, R213, R214 and R218—were each mutated to alanine to test whether they are involved in tRNA binding. Based on the EMSA experiments (Figure 6A), all of these four mutants, *Ec*TrmJ-K211A, *Ec*TrmJ-R213A, *Ec*TrmJ-R214A and *Ec*TrmJ-R218A, show largely reduced tRNA binding affinity compared with wild-type *Ec*TrmJ. Consistently, all

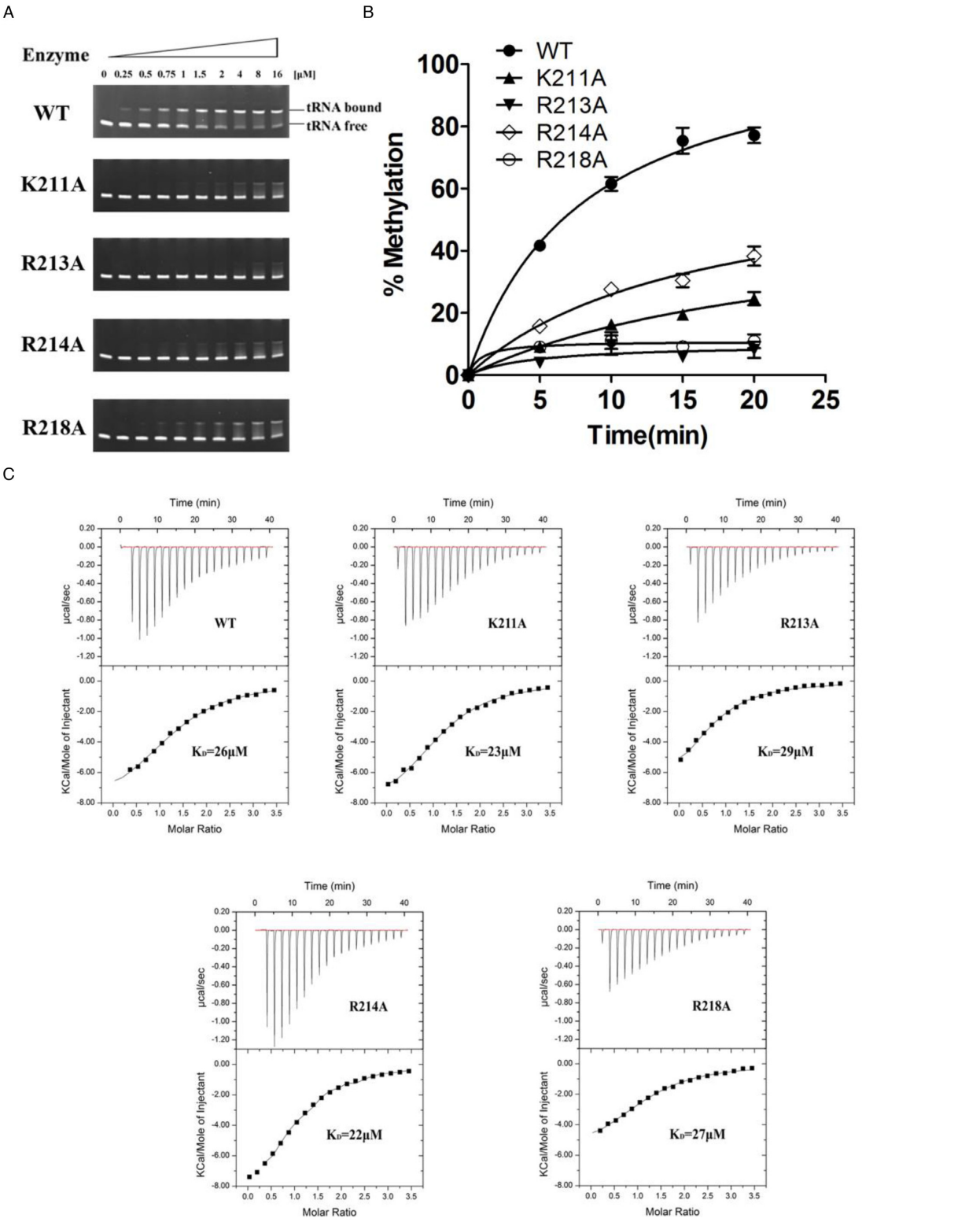

Figure 6. Ala mutations of protein surface basic amino acid residues in the CTD of *Ec*TrmJ. (**A**) The binding affinities of *Ec*TrmJs for *Ec*tRNA$_f^{Met}{}_1$ were analyzed by EMSA. (**B**) The methyltransferase activities of *Ec*TrmJ variants. Error bars represent standard errors of three independent experiments. (**C**) The binding affinities for SAH by ITC.

Table 3. Data collection and refinement statistics

Escherichiacoli TrmJ	+SAH
Data collection	
Space group	$C222_1$
Cell dimensions	
a, b, c (Å)	113.86, 136.57, 99.61
α, β, γ (°)	90.00, 90.00, 90.00
Resolution (Å)[a]	50.00–2.60 (2.69–2.60)
R_{merge}	0.15 (0.64)
I/σI	19.4 (3.9)
Completeness (%)	99.9 (100.0)
Redundancy	7.2 (6.9)
Refinement	
Resolution (Å)	38.9–2.60
No. reflections work/free	24353/1239
R_{work}/R_{free}	0.19/0.24
No. atoms	
Protein	3498 (2 subunits)
Ligand	52 (2*SAH)
Water/other	99
B-factors	
Protein	48.4
Ligand	42.1
Water/other	44.3
R.M.S. deviations	
Bond lengths (Å)	0.009
Bond angles (°)	1.203

four Ala mutants showed reduced methyltransferase activity and strikingly *Ec*TrmJ-R213A showed no detectable catalytic activity (Figure 6B). The steady-state kinetic parameters were measured for those mutants and yielded K_m values of *Ec*TrmJ-K211A, *Ec*TrmJ-R214A and *Ec*TrmJ-R218A, for tRNA that were ∼8- to 20-fold higher than that of wild-type *Ec*TrmJ, while the respective k_{cat} values did not change significantly (Table 4). These kinetic data suggest that the loss of catalytic activity in these mutants was a consequence of their low affinity for tRNA and this finding was consistent with the EMSA results. To further exclude the possibility that residues K211, R213, R214 and R218 were involved in SAM/SAH binding, the SAH binding affinities were assayed by ITC for all of these Ala mutants. As shown in Figure 6C, all four mutants, *Ec*TrmJ-K211A, *Ec*TrmJ-R213A, *Ec*TrmJ-R214A and *Ec*TrmJ-R218A, exhibited comparable K_D of SAH values as *Ec*TrmJ.

Collectively, these results suggest that the large positively charged surface patch in the CTD that includes residues K211, R213, R214 and R218 is important for tRNA binding to *Ec*TrmJ. Indeed, these four basic residues are highly conserved among bacterial TrmJs (Figure 3C), with R214 and R218 being strictly conserved, and K211 and R213 being relatively conserved with basic residues K or R in those sites.

Activity of isolated NTD and CTD, and the critical role of the flexible linker connecting these two domains

Based on these above investigations, residues from both the NTD (i.e. encompassing the SPOUT fold) and CTD are involved in tRNA binding to *Ec*TrmJ. As expected, the isolated NTD and CTD alone could not bind to substrate tRNAs (Figure 7A). Moreover, a mixture of isolated NTD with half of the linker sequence (residues 1–170) and the CTD with the other half of the linker (residues 171–246) could not bind tRNAs (Figure 7A). Similarly, isolated NTD alone or together with CTD do not show any detectable methyltransferase activity (Figure 7B), although NTD alone could bind SAH as effectively as full-length *Ec*TrmJ (Supplementary Figure S3).

We further investigated the function of the linker polypeptide (residues 164–179) that connects the NTD and CTD in *Ec*TrmJ. This linker does not show sequence conservation in bacterial TrmJs, but varies in length from 16 to 21 amino acid residues (Figure 3C). Thus, residues with $–NH_2$ or –OH groups in their side chain (H172, T175 and Y177) that could potentially make contact with tRNA substrates were mutated into alanine. However, none of these mutations altered the methyltransferase activity of *Ec*TrmJ (Figure 7C). Subsequently, we shortened the length of the linker in a stepwise manner. When two or four residues were deleted, there was no defect in the methyltransferase activity of *Ec*TrmJ (Figure 7D); however, when seven or more residues were deleted, the mutated *Ec*TrmJs totally lost methyltransferase activity (Figure 7D). Overall, these results show that the linker region plays critical roles in the methyl-transfer process of *Ec*TrmJ.

DISCUSSION

Residues involved in tRNA binding and a proposed tRNA-bound model of *Ec*TrmJ

A previous study demonstrated that *Ec*TrmJ requires a full-length tRNA as a substrate and discriminates the D-stem/loop (39). In this present study, we further showed that the L-shape tertiary structure of tRNA is essential for recognition by *Ec*TrmJ, while the amino acid acceptor stem is not involved in this process. However, the intriguing question of how *Ec*TrmJ recognizes its tRNA substrates remains unanswered. Based on a crystallographic analysis of *Ec*TrmJ, we made Ala mutations of many basic residues on the protein surface. Based on our EMSA, ITC and enzymatic results, we found that residues from both the catalytic NTD and extensional CTD of *Ec*TrmJ were involved in tRNA binding. Specifically, those residues were the two conserved arginine residues (R82 and R84) from the bacterial 'TrmJ-specific motif' in the NTD and four conserved positively charged residues (K211, R213, R214 and R218) from helix a8 in the CTD. The bacterial 'TrmJ-specific motif' is the first half of loop β4–α4 with a consensus 'TXARXR' sequence (Figure 3C). This motif plays an important role in the catalytic activity of *Ec*TrmJ, the first three residues 'TSA' all directly interact with SAH (Figure 4A and B) and the following R82 and R84 residues govern binding with tRNA substrates. This 'TXARXR' sequence is extremely conserved in bacterial TrmJs (Figure 3C), which suggests that the function of this 'TrmJ-specific motif' in SAM/SAH and tRNA binding is common to all bacterial TrmJs. The protein sequence of CTD is less conserved than that of the SPOUT NTD in TrmJs (Figure 3C), but the few conserved residues in the CTD were either located at the protein dimer interface or were involved in binding to tRNAs. Hence, we proposed that the mode of tRNA binding with CTD is also conserved in bacterial TrmJs.

*Ec*TrmJ recognizes the D-stem/loop and elbow region of tRNA, and catalyzes the methyltransfer reaction at the

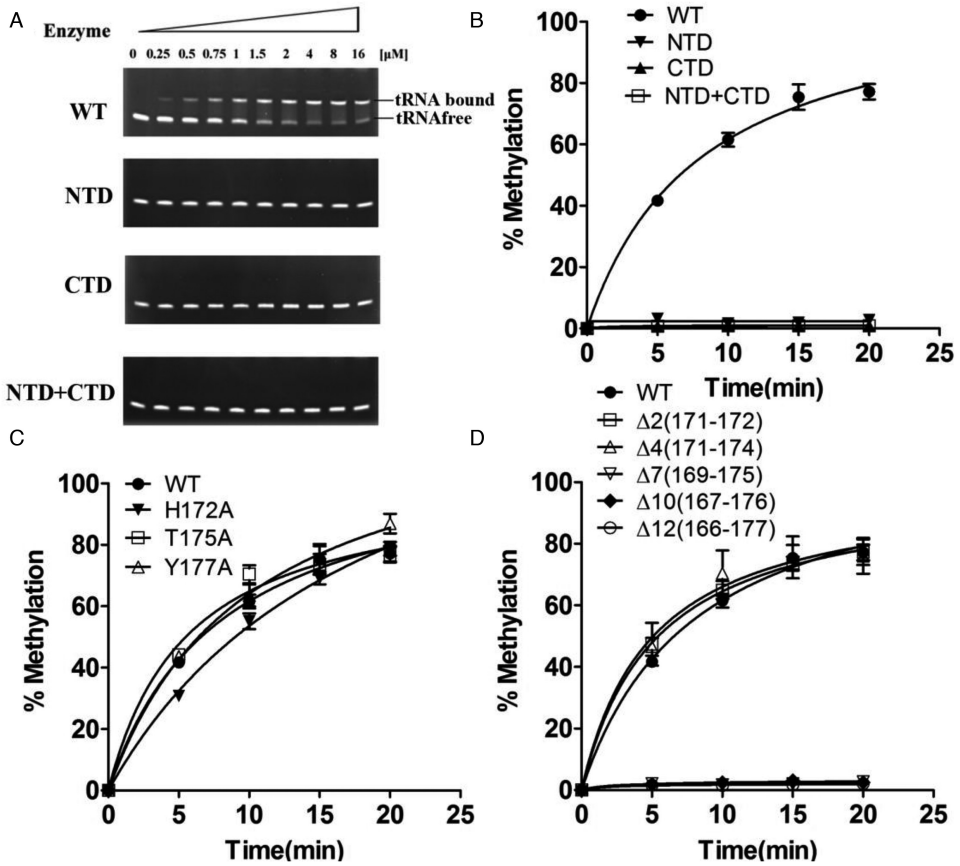

Figure 7. Roles of the hinge region that connect the NTD and CTD. (**A**) The tRNA binding affinities of the isolated NTD and CTD were analyzed by EMSA. (**B**) The methyltransferase activities of the isolated NTD and CTD. (**C** and **D**) The methyltransferase activities of *Ec*TrmJ variants in the hinge region. The NTD and CTD in this figure are domains with residues from 1–170 and 171–246, respectively. Error bars represent standard errors of three independent experiments.

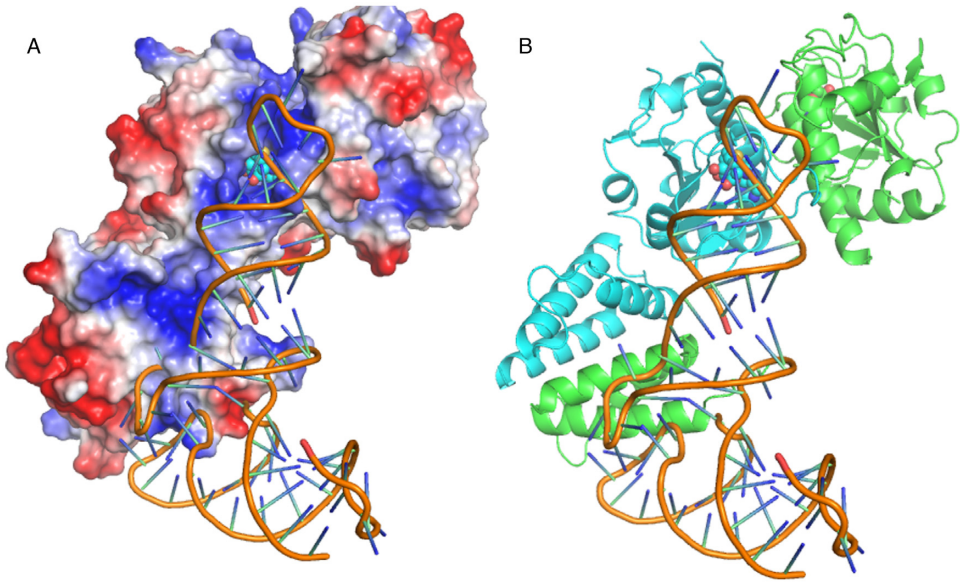

Figure 8. A proposed model of tRNA binding to *Ec*TrmJ. (**A** and **B**) Proposed models of the *Ec*TrmJ dimer bound with one tRNA substrate in the same view; the tRNA backbone is shown in orange.

Table 4. Kinetic parameters of wild-type and mutant *Ec*TrmJs

*Ec*TrmJ variants	K_m (μM)	k_{cat} (min^{-1})	k_{cat}/K_m (relative)
wild-type	0.67 ± 0.06	1.52 ± 0.08	1
R115A	0.63 ± 0.11	1.44 ± 0.14	1.01
K211A	13.76 ± 1.62	1.16 ± 0.08	0.04
R213A	ND	ND	ND
R214A	12.31 ± 1.86	1.82 ± 0.21	0.06
R218A	5.43 ± 0.20	1.11 ± 0.01	0.09

Data indicate means from three independent measurements; ND, not detected.

ASL region. In the crystal structure (Figure 3A), *Ec*TrmJ presents as an asymmetric dimer. The relative orientation between CTD and NTD differed between the two monomers (Figure 3B). The two positively charged patches of *Ec*TrmJ involved in tRNA binding in one subunit are too close to bind a tRNA substrate. By contrast, in the other subunit, the two patches are too far apart to bind tRNA (Figure 3A and B). Based on the conformation of *Ec*TrmJ in the crystal structure, we proposed a model of cross-subunit binding of tRNA for *Ec*TrmJ (Figure 8A and B). In this model, residues R82 and R84 near the SAM/SAH-binding pocket from the SPOUT domain make contact with the ASL of tRNA, while the D-stem/loop and elbow region of tRNA form contacts with the CTD. However, it is just a proposed model, the real situation of how *Ec*TrmJ binding with tRNA remains to be illuminated. Importantly, the linker region is flexible, so the possibility remains that the relative orientation between the CTD and NTD can change and differ from the current structure; also, there could be some conformations of *Ec*TrmJ that are more acceptable for binding to tRNA substrates.

For a decade, it has been thought that the N- and/or C-terminal extensions of SPOUT MTases include a key sequence to recognize substrate RNAs. The extensions are known to be involved in the binding of substrate tRNAs in all reported SPOUT MTases with extensions, such as TrmH (32,34) and TrmD (12). However, in those MTases, residues from the SPOUT catalytic domain are also involved in tRNA binding (12,32,34). Moreover, recent studies suggest that the SPOUT domain plays even more important roles in tRNA recognition than expected. One example is that TrmH discriminates between substrate and non-substrate tRNAs by the SPOUT domain instead of the extensional domains (34). The other example comes from the minimalist SPOUT MTase, TrmL, which can independently recognize and bind to substrate tRNAs by the SPOUT domain alone (18). In this present study of *Ec*TrmJ, both the SPOUT domain and extensional CTD were involved in the initial binding to tRNA, and our work further suggests that the delicate cooperation of those two domains through the hinge region is critical for tRNA recognition (Figure 7). Moreover, tRNA substrate discrimination might also need to be accomplished by these two domains acting together, because the domain exchange of CTDs between *Ec*TrmJ and *Sa*TrmJ only causes the inactivation of chimeric proteins (39).

The asymmetric dimer of *Ec*TrmJ

*Ec*TrmJ presents as a dimer in both the crystal structure and while in solution. Our crystal structure of *Ec*TrmJ showed that both the SPOUT domain and extensional CTD form separate dimers (Figure 3A). Indeed, except for the monomeric state of *Saccharomyces cerevisiae* Trm10 (52), dimer formation of the SPOUT domain occurs in all known SPOUT MTases (11–15,18). However, to the best of our knowledge, this is the first report of dimerization of the extensional domain. Ala mutations of residues at the dimer interface of the CTD largely reduce the enzymatic activity (Figure 4D), which suggests that dimerization of the CTD is important for *Ec*TrmJ function. The NTD and CTD are linked by a long, flexible hinge in each monomer, and the relative orientations between the CTD and NTD differed between the two monomers (Figure 3B), suggesting that *Ec*TrmJ is an asymmetric dimer. All other SPOUT MTases exist as symmetric dimers in their crystal structures (11–15,18), and those monomers from symmetric dimers are thought to have equal binding ability toward tRNA substrates. However, there is an absence of solid proof to support a model in which one SPOUT dimer can simultaneously bind to two tRNA molecules. Instead, the 'half-of-the-sites' reactivity of the dimer for tRNA binding and product synthesis was recently reported for *E. coli* TrmD in a pre-steady-state kinetics study (28). The capture of only one tRNA molecule by a SPOUT MTase dimer was also observed for *T. thermophilus* TrmH by gel-filtration analyses (31). Therefore, intriguing questions regarding how many tRNA substrates bind to one TrmJ dimer during the catalysis process remain elusive.

Conformational changes occur before the capture of tRNA substrates

For SPOUT tRNA MTases, such as TrmL (18) and TrmH (31), tRNA–enzyme complexes could be observed by EMSA, even without the presence of SAM or SAH, which suggests that apo enzymes can bind to substrate tRNAs. However, this was not the case for *Ec*TrmJ. Neither apo *Ec*TrmJ nor the *Ec*TrmJ–SAM (or *Ec*TrmJ–SAH) complex could form a stable complex with tRNA, as detected by EMSA. Such *Ec*TrmJ–tRNA complexes could only be observed in the presence of the SAM-dependent MTase inhibitor sinefungin. Sinefungin is a SAM analog that can bind to the SAM/SAH-binding pocket. One possibility is that the binding of SAM or SAH could introduce some conformational changes in *Ec*TrmJ that are essential for binding to tRNA substrates. Accordingly, this

conformational state could be stabilized by sinefungin because it is an inhibitor. No crystal structure of *Ec*TrmJ in the apo form or in complex with sinefungin is yet available, so we can only compare the structure of the *Ec*TrmJ–SAH complex described in this study with the apo form of the isolated *Ec*TrmJ SPOUT domain (PDB: 4CND) (39). The major structural differences in the SPOUT domain are derived from the β4–α4 loop, which includes the 'TrmJ-specific motif' that moves closer toward the active site after SAH binding. We can hypothesize that SAM/SAH binding by *Ec*TrmJ triggers conformational changes of the 'TrmJ-specific motif', which facilitates the binding of substrate tRNA molecules. Because tRNA binding by *Ec*TrmJ requires the cooperative influences of residues from both the NTD and CTD domains, and as these two domains are connected by a long, flexible hinge region, the possibility remains that SAM/SAH binding could cause even more dramatic conformational changes to accommodate substrate tRNAs. Obtaining a complete understanding of the underlying mechanism will require additional studies in the future.

ACCESSION NUMBERS

PDB IDs: 4XBO, 3ILK, 4CNE and 4CND.

SUPPLEMENTARY DATA

Supplementary Data are available at NAR Online.

ACKNOWLEDGEMENT

We gratefully acknowledge Prof. Richard Giegé for carefully reading the manuscript and important discussion.

FUNDING

The Natural Science Foundation of China [31130064, 31270775, 81471113]; National Key Basic Research Foundation of China [2012CB911000]; Committee of Science and Technology in Shanghai [12JC1409700]. Funding for open access charge: The Natural Science Foundation of China [31130064, 31270775, 81471113]; National Key Basic Research Foundation of China [2012CB911000]; Committee of Science and Technology in Shanghai [12JC1409700].
Conflict of interest statement. None declared.

REFERENCES

1. El Yacoubi,B., Bailly,M. and de Crécy-Lagard,V. (2012) Biosynthesis and function of posttranscriptional modifications of transfer RNAs. *Annu. Rev. Genet.*, **46**, 69–95.
2. Grosjean,H. (2009) *DNA and RNA Modification Enzymes: Structure, Mechanism, Function and Evolution*. Landes Bioscience, Austin, TX.
3. Phizicky,E.M. and Hopper,A.K. (2010) tRNA biology charges to the front. *Genes Dev.*, **24**, 1832–1860.
4. Machnicka,M.A., Milanowska,K., Osman Oglou,O., Purta,E., Kurkowska,M., Olchowik,A., Januszewski,W., Kalinowski,S., Dunin-Horkawicz,S., Rother,K.M. *et al.* (2013) MODOMICS: a database of RNA modification pathways–2013 update. *Nucleic Acids Res.*, **41**, D262–D267.
5. Cantara,W.A., Crain,P.F., Rozenski,J., McCloskey,J.A., Harris,K.A., Zhang,X., Vendeix,F.A., Fabris,D. and Agris,P.F. (2011) The RNA Modification Database, RNAMDB: 2011 update. *Nucleic Acids Res.*, **39**, D195–D201.
6. Jühling,F., Mörl,M., Hartmann,R.K., Sprinzl,M., Stadler,P.F. and Pütz,J. (2009) tRNAdb 2009: compilation of tRNA sequences and tRNA genes. *Nucleic Acids Res.*, **37**, D159–D162.
7. Agris,P.F. (2008) Bringing order to translation: the contributions of transfer RNA anticodon-domain modifications. *EMBO Rep.*, **9**, 629–635.
8. Giegé,R. and Eriani,G. (2014) *Transfer RNA Recognition and Aminoacylation by Synthetases.* John Wiley & Sons, Chichester.
9. Hori,H. (2014) Methylated nucleosides in tRNA and tRNA methyltransferases. *Front. Genet.*, **5**, 144.
10. Anantharaman,V., Koonin,E.V. and Aravind,L. (2002) SPOUT: a class of methyltransferases that includes spoU and trmD RNA methylase superfamilies, and novel superfamilies of predicted prokaryotic RNA methylases. *J. Mol. Microbiol. Biotechnol.*, **4**, 71–75.
11. Ahn,H.J., Kim,H.W., Yoon,H.J., Lee,B.I., Suh,S.W. and Yang,J.K. (2003) Crystal structure of tRNA(m1G37)methyltransferase: insights into tRNA recognition. *EMBO J.*, **22**, 2593–2603.
12. Elkins,P.A., Watts,J.M., Zalacain,M., van Thiel,A., Vitazka,P.R., Redlak,M., Andraos-Selim,C., Rastinejad,F. and Holmes,W.M. (2003) Insights into catalysis by a knotted TrmD tRNA methyltransferase. *J. Mol. Biol.*, **333**, 931–949.
13. Liu,J., Wang,W., Shin,D.H., Yokota,H., Kim,R. and Kim,S.H. (2003) Crystal structure of tRNA (m1G37) methyltransferase from *Aquifex aeolicus* at 2.6 Å resolution: a novel methyltransferase fold. *Proteins*, **53**, 326–328.
14. Lim,K., Zhang,H., Tempczyk,A., Krajewski,W., Bonander,N., Toedt,J., Howard,A., Eisenstein,E. and Herzberg,O. (2003) Structure of the YibK methyltransferase from *Haemophilus influenzae* (HI0766): a cofactor bound at a site formed by a knot. *Proteins*, **51**, 56–67.
15. Nureki,O., Watanabe,K., Fukai,S., Ishii,R., Endo,Y., Hori,H. and Yokoyama,S. (2004) Deep knot structure for construction of active site and cofactor binding site of tRNA modification enzyme. *Structure*, **12**, 593–602.
16. Tkaczuk,K.L., Dunin-Horkawicz,S., Purta,E. and Bujnicki,J.M. (2007) Structural and evolutionary bioinformatics of the SPOUT superfamily of methyltransferases. *BMC Bioinformatics*, **8**, 73.
17. Benítez-Páez,A., Villarroya,M., Douthwaite,S., Gabaldon,T. and Armengod,M.E. (2010) YibK is the 2′-O-methyltransferase TrmL that modifies the wobble nucleotide in *Escherichia coli* tRNA(Leu) isoacceptors. *RNA*, **16**, 2131–2143.
18. Liu,R.J., Zhou,M., Fang,Z.P., Wang,M., Zhou,X.L. and Wang,E.D. (2013) The tRNA recognition mechanism of the minimalist SPOUT methyltransferase, TrmL. *Nucleic Acids Res.*, **41**, 7828–7842.
19. Purta,E., Kaminska,K.H., Kasprzak,J.M., Bujnicki,J.M. and Douthwaite,S. (2008) YbeA is the m3Psi methyltransferase RlmH that targets nucleotide 1915 in 23S rRNA. *RNA*, **14**, 2234–2244.
20. Ero,R., Leppik,M., Liiv,A. and Remme,J. (2010) Specificity and kinetics of 23S rRNA modification enzymes RlmH and RluD. *RNA*, **16**, 2075–2084.
21. Clouet-d'Orval,B., Gaspin,C. and Mougin,A. (2005) Two different mechanisms for tRNA ribose methylation in Archaea: a short survey. *Biochimie*, **87**, 889–895.
22. Reichow,S.L., Hamma,T., Ferré-D'Amaré,A.R. and Varani,G. (2007) The structure and function of small nucleolar ribonucleoproteins. *Nucleic Acids Res.*, **35**, 1452–1464.
23. Ziesche,S.M., Omer,A.D. and Dennis,P.P. (2004) RNA-guided nucleotide modification of ribosomal and non-ribosomal RNAs in Archaea. *Mol. Microbiol.*, **54**, 980–993.
24. Renalier,M.H., Joseph,N., Gaspin,C., Thebault,P. and Mougin,A. (2005) The Cm56 tRNA modification in archaea is catalyzed either by a specific 2′-O-methylase, or a C/D sRNP. *RNA*, **11**, 1051–1063.
25. Björk,G.R., Jacobsson,K., Nilsson,K., Johansson,M.J., Byström,A.S. and Persson,O.P. (2001) A primordial tRNA modification required for the evolution of life? *EMBO J.*, **20**, 231–239.
26. Brulé,H., Elliott,M., Redlak,M., Zehner,Z.E. and Holmes,W.M. (2004) Isolation and characterization of the human tRNA-(N1G37) methyltransferase (TRM5) and comparison to the *Escherichia coli* TrmD protein. *Biochemistry*, **43**, 9243–9255.
27. Christian,T. and Hou,Y.M. (2007) Distinct determinants of tRNA recognition by the TrmD and Trm5 methyl transferases. *J. Mol. Biol.*, **373**, 623–632.

28. Christian,T., Lahoud,G., Liu,C. and Hou,Y.M. (2010) Control of catalytic cycle by a pair of analogous tRNA modification enzymes. *J. Mol. Biol.*, **400**, 204–217.
29. Lahoud,G., Goto-Ito,S., Yoshida,K., Ito,T., Yokoyama,S. and Hou,Y.M. (2011) Differentiating analogous tRNA methyltransferases by fragments of the methyl donor. *RNA*, **17**, 1236–1246.
30. Sakaguchi,R., Giessing,A., Dai,Q., Lahoud,G., Liutkeviciute,Z., Klimasauskas,S., Piccirilli,J., Kirpekar,F. and Hou,Y.M. (2012) Recognition of guanosine by dissimilar tRNA methyltransferases. *RNA*, **18**, 1687–1701.
31. Watanabe,K., Nureki,O., Fukai,S., Ishii,R., Okamoto,H., Yokoyama,S., Endo,Y. and Hori,H. (2005) Roles of conserved amino acid sequence motifs in the SpoU (TrmH) RNA methyltransferase family. *J. Biol. Chem.*, **280**, 10368–10377.
32. Watanabe,K., Nureki,O., Fukai,S., Endo,Y. and Hori,H. (2006) Functional categorization of the conserved basic amino acid residues in TrmH (tRNA (Gm18) methyltransferase) enzymes. *J. Biol. Chem.*, **281**, 34630–34639.
33. Ochi,A., Makabe,K., Kuwajima,K. and Hori,H. (2010) Flexible recognition of the tRNA G18 methylation target site by TrmH methyltransferase through first binding and induced fit processes. *J. Biol. Chem.*, **285**, 9018–9029.
34. Ochi,A., Makabe,K., Yamagami,R., Hirata,A., Sakaguchi,R., Hou,Y.M., Watanabe,K., Nureki,O., Kuwajima,K. and Hori,H. (2013) The catalytic domain of topological knot tRNA methyltransferase (TrmH) discriminates between substrate tRNA and nonsubstrate tRNA via an induced-fit process. *J. Biol. Chem.*, **288**, 25562–25574.
35. Pintard,L., Lecointe,F., Bujnicki,J.M., Bonnerot,C., Grosjean,H. and Lapeyre,B. (2002) Trm7p catalyses the formation of two 2′-O-methylriboses in yeast tRNA anticodon loop. *EMBO J.*, **21**, 1811–1820.
36. Guy,M.P., Podyma,B.M., Preston,M.A., Shaheen,H.H., Krivos,K.L., Limbach,P.A., Hopper,A.K. and Phizicky,E.M. (2012) Yeast Trm7 interacts with distinct proteins for critical modifications of the tRNAPhe anticodon loop. *RNA*, **18**, 1921–1933.
37. Guy,M.P. and Phizicky,E.M. (2015) Conservation of an intricate circuit for crucial modifications of the $tRNA^{Phe}$ anticodon loop in eukaryotes. *RNA*, **21**, 61–74.
38. Purta,E., van Vliet,F., Tkaczuk,K.L., Dunin-Horkawicz,S., Mori,H., Droogmans,L. and Bujnicki,J.M. (2006) The yfhQ gene of *Escherichia coli* encodes a tRNA:Cm32/Um32 methyltransferase. *BMC Mol. Biol.*, **7**, 23.
39. Somme,J., Van Laer,B., Roovers,M., Steyaert,J., Versées,W. and Droogmans,L. (2014) Characterization of two homologous 2′-O-methyltransferases showing different specificities for their tRNA substrates. *RNA*, **20**, 1257–1271.
40. Hori,H., Saneyoshi,M., Kumagai,I., Miura,K. and Watanabe,K. (1989) Effects of modification of 4-thiouridine in *E. coli* tRNA(fMet) on its methyl acceptor activity by thermostable Gm-methylases. *J. Biochem.*, **106**, 798–802.
41. Zhou,M., Long,T., Fang,Z.P., Zhou,X.L., Liu,R.J. and Wang,E.D. (2015) Identification of determinants for tRNA substrate recognition by *Escherichia coli* C/U34 2′-O-methyltransferase. *RNA Biol.*, doi:10.1080/15476286.2015.1050576.
42. Gill,S.C. and von Hippel,P.H. (1989) Calculation of protein extinction coefficients from amino acid sequence data. *Anal. Biochem.*, **182**, 319–326.
43. Kibbe,W.A. (2007) OligoCalc: an online oligonucleotide properties calculator. *Nucleic Acids Res.*, **35**, W43–W46.
44. Otwinowski,Z. and Minor,W. (1997) Processing of X-ray diffraction data collected in oscillation mode. *Methods Enzymol.*, **276**, 307–326.
45. McCoy,A.J., Grosse-Kunstleve,R.W., Adams,P.D., Winn,M.D., Storoni,L.C. and Read,R.J. (2007) Phaser crystallographic software. *J. Appl. Crystallogr.*, **40**, 658–674.
46. Bailey,S. (1994) The CCP4 suite: programs for protein crystallography. *Acta. Crystallogr. D. Biol. Crystallogr.*, **50**, 760–763.
47. Adams,P.D., Grosse-Kunstleve,R.W., Hung,L.W., Ioerger,T.R., McCoy,A.J., Moriarty,N.W., Read,R.J., Sacchettini,J.C., Sauter,N.K. and Terwilliger,T.C. (2002) PHENIX: building new software for automated crystallographic structure determination. *Acta. Crystallogr. D. Biol. Crystallogr.*, **58**, 1948–1954.
48. Emsley,P. and Cowtan,K. (2004) Coot: model-building tools for molecular graphics. *Acta. Crystallogr. D. Biol. Crystallogr.*, **60**, 2126–2132.
49. Murshudov,G.N., Vagin,A.A. and Dodson,E.J. (1997) Refinement of macromolecular structures by the maximum-likelihood method. *Acta. Crystallogr. D. Biol. Crystallogr.*, **53**, 240–255.
50. Laskowski,R.A., MacArthur,M.W., Moss,D.S. and Thornton,J.M. (1993) PROCHECK: a program to check the stereochemical quality of protein structures. *J. Appl. Crystallogr.*, **26**, 283–291.
51. Robert,X. and Gouet,P. (2014) Deciphering key features in protein structures with the new ENDscript server. *Nucleic Acids Res.*, **42**, W320–W324.
52. Shao,Z., Yan,W., Peng,J., Zuo,X., Zou,Y., Li,F., Gong,D., Ma,R., Wu,J., Shi,Y. *et al.* (2014) Crystal structure of tRNA m1G9 methyltransferase Trm10: insight into the catalytic mechanism and recognition of tRNA substrate. *Nucleic Acids Res.*, **42**, 509–525.